International Journal of Coal Geology 193 (2018) 61–72

Contents lists available at ScienceDirect

International Journal of Coal Geology

journal homepage: www.elsevier.com/locate/coal

A dynamic-pulse pseudo-pressure method to determine shale matrix permeability at representative reservoir conditions

Kunkun Fan[a,c], Mingzhe Dong[a,b,*], Derek Elsworth[c], Yajun Li[a], Congbin Yin[d], Yanchao Li[d]

[a] College of Petroleum Engineering, China University of Petroleum, Qingdao 266555, China
[b] Department of Chemical and Petroleum Engineering, University of Calgary, Calgary, AB T2N 1N4, Canada
[c] Energy and Mineral Engineering, Pennsylvania State University, University Park, PA 16801, USA
[d] Downhole Service Company, Chuanqing Drilling Company, CNPC, Chengdu 610051, China

ARTICLE INFO

Keywords:
Shale
Matrix permeability
Gas dynamic production
Spherical model
Pseudo pressure

ABSTRACT

Matrix permeability is a key factor in determining long term gas production from shale reservoirs – requiring that it is determined under true reservoir conditions. We suggest a variable pressure gradient (VPG) protocol to measure shale matrix permeability using real reservoir fluids in powdered samples. The VPG method is described and a mathematical protocol for its analysis is developed. The first measures gas fractional production rate history under constant external pressure for each production stage and with a designated pressure gradient. The second establishes the mathematical protocol for analysis using pseudo-pressure to accommodate both the effect of gas pressure-dependent PVT parameters and desorption rate coefficient. The matrix permeability is determined by matching the solution of the model with the experimental data. The model fits the experimental data well when the fractional production is < 0.75. Shale matrix permeability is calculated in the order of magnitude of 10^{-7}–10^{-6} md. Methane permeability decreases with a decrease in both average pore pressure and particle size of the individual component grains. Permeability considerably more sensitive to changes in desorption rate coefficient than flow regimes. Compared with current small pressure gradient (SPG) methods, the VPG method is considerably more applicable to actual gas production and reduces to the SPG method under simplified boundary conditions. Although some approximate treatments are used for establishing the VPG method and some flow mechanisms are not considered, this study still provides an information-rich technique to determine shale matrix permeability at conditions close to reality.

1. Introduction

Shale gas reservoirs provide an enormous potential resource for world energy supply (Bustin and Bustin, 2012; Chen et al., 2011; Hartwig et al., 2009), but suffer considerable challenges in production – including ultralow permeability (in the range of 10^{-3}–10^{-7} md), small porosity (2–8%), and the unknown response of rich components of organic matter and clay minerals (Sang et al., 2016a, 2016b; Wang et al., 2016b). Advanced technologies such as horizontal drilling and multi-staged hydraulic fracturing have allowed commercial production of shale gas, but concerns still exist regarding limitations of available tools to forecast gas production and approaches to maintain long-term economic production (Ding et al., 2012; Dubost, 2012). Gas transport in fractured shale formations is a complex multi-stage process, including gas flow from pore to micro fractures, from micro fractures to artificial fractures and from artificial fractures to the well. The stimulated reservoir volume created by fluid-driven (hydraulic) fracturing is very small compared to the total target reservoir (Song and Ehlig-Economides, 2011) with the gas mainly stored in the matrix by physical adsorption(Gasparik et al., 2012; Li and Wu, 2015; Rexer et al., 2013; Ross et al., 2012; Yu et al., 2016; Zapata and Sakhaee-Pour, 2016). Thus, gas flow characteristics from the shale matrix to fractures are of significant importance in evaluating long term gas production and prediction - making shale matrix permeability a key factor in evaluating gas production.

Simple models for Darcy flow do not correctly describe the behavior of gas flow in shale formations. Many conceptual models have been established to correct the gas flow behaviors for three principal mechanisms - including molecular diffusion, Knudsen diffusion and surface diffusion (Carlson and Mercer, 1991; Fathi et al., 2012; Freeman et al., 2011; Javadpour, 2009; Javadpour et al., 2007; Kazemi and Borujeni, 2015; Klinkenberg, 1941; Okamoto et al., 2015; Ozkan et al., 2010; Singh et al., 2014; Sondergeld et al., 2010; Wu et al., 2014). Boundaries between these different flow regimes are often scaled relative to

* Corresponding author at: College of Petroleum Engineering, China University of Petroleum, Qingdao 266555, China.
E-mail address: Mingzhe.dong@ucalgary.ca (M. Dong).

https://doi.org/10.1016/j.coal.2018.04.011
Received 29 December 2017; Received in revised form 22 April 2018; Accepted 24 April 2018
Available online 25 April 2018

Knudsen number, a dimensionless number defined as the ratio of the molecular mean free path to the average pore diameter. The larger the value of the Knudsen number, the closer the flow conforms to molecular diffusion. Conversely, the smaller the Knudsen number, the closer the flow is to continuous flow. Other concerns in making reliable permeability measurements include issues related to: gas adsorption/desorption (Sakhaee-Pour and Bryant, 2011); flow anisotropy (Milner et al., 2010); pore wettability (Milner et al., 2010); and the influence of natural fractures (Azom and Javadpour, 2012). Despite corrections for some of these gas flow mechanisms, magnitudes of permeability recovered from some conceptual models remain inconsistent and their validity must be confirmed by experimental or field production data.

Typical methods of permeability measurements are using steady state (SS), un-steady state (USS) and pressure oscillation (PO) methods. In the SS method, gas is injected at either constant pressure gradient or constant flow rate along the core axis until equilibrium state is achieved (API, 1998). The typical disadvantage is the extended duration of the test for ultralow permeability media. When applying the USS method, permeability is deduced from the decay of a pressure pulse applied to the upstream or downstream face of the sample (Bourbie and Walls, 1982; Brace et al., 1968; Dicker and Smits, 1988; Guo et al., 2015; Hsieh et al., 1981; Jones, 1972; Lin, 1977; Luffel et al., 1993; Neuzil et al., 1981; Qu et al., 2015; Suarez-Rivera et al., 2012; Van-Oort, 1994; Yang et al., 2015; Yang and Dong, 2017). In order to reduce the effect of coring-induced micro-fractures on the measured (matrix) permeability, these methods may also be applied to powdered samples (Cui et al., 2009; Egermann et al., 2002; Handwerger et al., 2011; Luffel et al., 1993) – thus significantly reducing the duration of each permeability measurement. Disadvantages are that it is subject to a priori assumptions (that gas PVT parameters are constant) in establishing flow models and that the measured data are sensitive to some petrophysical parameters. The PO method can be considered as a hybrid of SS and USS measurements, where permeability is deduced from the amplitude attenuation and phase shift of the applied signal (Bernabé et al., 2006; Egermann et al., 2002; Fischer, 1992). This method can increase the sensitivity of the measurements but the frequency of the oscillation influences the depth of penetration into the powdered samples and can limit the representativeness of the sampled permeability.

Among these three different methods, the USS method has been most fully developed and has become the principal method to determine the permeability of tight formations since first presented (Brace et al., 1968). In principle, the method is similar to well testing, and a large number of studies focus on optimizing the volume of upstream and downstream reservoirs (or boundaries of the mathematical models) to balance measurement sensitivity to experimental duration. However, current USS methods are conducted using only a small pressure gradient (SPG) and the solutions are obtained on the basis of constant gas PVT properties. This may lead to significantly erroneous results when applied to actual field production with variable pressure gradients (VPG) (Al-Hussainy et al., 1966; Fraim and Wattenbarger, 1987) and variations in pressure-dependent viscosities and compressibilities cannot be ignored. To our knowledge, no methods are provided to describe response in the presence of variable and significant pressure gradients.

The following provides a protocol to determine shale matrix permeability under variable pressure gradients on powdered shale samples. First, static methane adsorption/desorption isotherms are obtained experimentally and the Langmuir parameters are calculated. Second, dynamic desorption-flow production tests are conducted under constant external pressure in stepped-pressure production stages with a designated pressure gradient. Third, a mathematical model accommodating desorption for spherical flow in individual representative particles is presented. Both general and approximate solutions are obtained by using the average methane desorption rate and the concept of pseudo pressure to accommodate the effect of variations of pressure-dependent viscosity and compressibility. A workflow for the VPG method is presented to determine shale permeability of powdered samples. Finally, the method is validated by comparisons with the SPG method. The applicability and limitations of the method as applied to field production are also discussed.

2. Experiment and theory

We define a new experimental procedure to scale dynamic gas production using powdered samples that utilizes gas pressures over large ranges representative of reservoir conditions. For these broad ranges of PVT conditions we utilize pseudo-pressures to accurately accommodate variations in fluid behavior in a straightforward but rigorous method of analysis.

2.1. Static and dynamic experiments

Gas production is controlled by various physical parameters relating to adsorption/desorption and permeability that together define rates of recovery at reservoir conditions.

2.1.1. Sample collection and characterization

Shale samples used in this work are collected from the Fuling shale play, southeast of Chongqing, Sichuan, China - a primary pilot experimentation area for shale gas production in China. Samples are crushed to three different size consists: 10–20 mesh, 60–80 mesh and 100–120 mesh. Pore characteristics are studied through liquid nitrogen adsorption tests with specific surface area determined via BET (Brunauer-Emmett-Teller) theory (Brunauer et al., 1938). Pore diameter and pore volume are calculated based on the BJH (Barrett-Joyner-Halenda) model (Barrett et al., 1951; Clarkson et al., 2013; Groen et al., 2003). The dominant mineral components are analyzed by X-ray diffraction. We assume that individual particles are spherical and that the constituent pores (in these spherical particles) are cylindrical (Fig. 1). The porosity and skeletal density of the sample can be approximately calculated from geometrical dimensions and mass. Physical and geochemical parameters of the particular sample are as listed in Table 1.

2.1.2. Static adsorption/desorption experiments

Dry powdered samples are used for the adsorption and desorption experiments. The samples are heated to 105 °C over three days, then vacuum desaturated for four hours (to an absolute pressure of $\sim 10^{-3}$ Pa) to remove moisture. The samples are then saturated with methane (reagent grade at 99.99% pure) at 1 atm prior to the initiation of the gas adsorption/desorption tests. The adsorption/desorption isotherms are obtained at 35 °C using the constant-volume method similar to those presented elswhere (Chen et al., 2011; Gasparik et al., 2012; Rexer et al., 2013; Ross et al., 2012; Yuan et al., 2014; Zhai et al., 2014).

2.1.3. Dynamic production experiments

Experiments for dynamic production of methane are conducted when the system pressure is decreased using three different pressure gradients. Magnitudes of the pressure gradients are determined

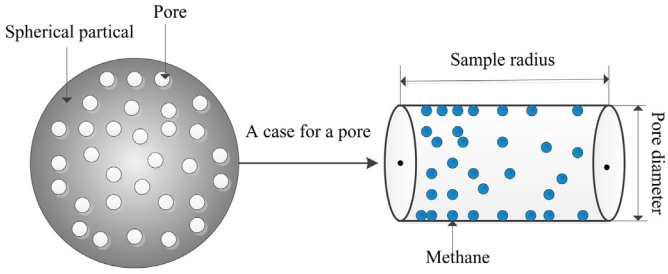

Fig. 1. Conceptual model of shale gas transport.

Table 1
Petrophysical and geochemical characteristics of shale sample.

Parameter	TOC (wt%)	Specific surface area (m^2/g)	Pore volume (10^{-3} cm^3/g)	Skeleton density (cm^3/g)
Value	2.81	2.55	16.37	2.80
Parameter	Porosity (%)	Average pore radius (10^{-3} μm)	Clay content (wt%)	Sample diameter (μm)
Value	4.39	25.68	18.28	215

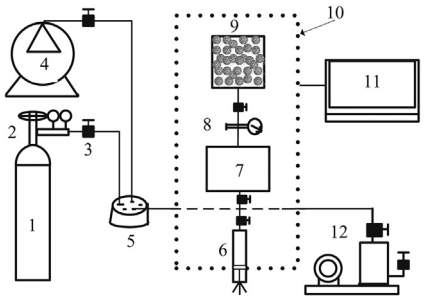

1- Gas source
2- Pressure regulator
3- Valve
4-Booster pump
5- Six-way valve
6- Volume controlled pump
7- Standard chamber
8-Precision pressure sensor
9-Sample chamber
10- Temperature-controlled system
11-Computer
12- Vacuum pump

Fig. 2. Experimental apparatus for dynamic gas production experiments.

according to the desorption isotherm – as presented later. All experiments are at a temperature of 35 °C and on shale of three distinct particle sizes (10–20 mesh, 60–80 mesh, 100–120 mesh). A schematic diagram of the dynamic desorption-diffusion apparatus is shown in Fig. 2.

Key components of the apparatus comprise a sample chamber, a standard chamber and a measuring pump. By using the measuring pump, the production pressure can be maintained constant for each production stage, and the gas production with time can be measured. The accuracy of the measuring pump to compensate for the volume of produced gas is ± 2.6 μL. Pressure sensors (Honeywell, USA) are used to record pressures in the standard chamber with a resolution of ± 6.9 10^{-4} MPa and an accuracy of ± 0.065%. System temperature is controlled by water bath and thermostat (accuracy of 0.01 °C) containing both the standard chamber and the sample chamber. This design guarantees the accuracy of the experimental apparatus.

Prior to conducting measurements, volume correction and leakage tests are conducted for the entire system using helium. The powdered samples are compacted into the sample chamber and void volume of the sample chamber is measured via PVT with helium. The entire experimental system is then evacuated for 12 h with the samples then saturated with methane (reagent grade 99.99% pure) at 1 atm. The following procedure is then applied for each measurement:

(1) Set the thermostat and water bath to the desired experimental temperature. Open the valve connecting the standard chamber and gas cylinder. Introduce methane into the standard chamber. Wait for > 1 h for the temperature of the system to stabilize at the desired test temperature. Record the pressure P_1 of the standard chamber.
(2) Connect the standard chamber to allow methane to flow into the sample chamber and be adsorbed in the shale samples. Wait for > 1 day for the pressure of the experimental system to stabilize at the test pressure. During the equilibrium process, set the system pressure close to the designed test pressure. When gas flow and adsorption in the shale samples equilibrates and the system pressure stabilizes, record the initial balance pressure P_2 and the volume change with time. This completes the preparation for adsorption.
(3) If the system pressure does not reach the designated test pressure, then boost the pressure with the pump until the highest pressure (up to 30 MPa) is reached and repeat steps (1) and (2).
(4) Isolate the standard chamber from the sample chamber and release some gas from the standard chamber. Then seal the standard chamber, record the corresponding pressure P_3. A pressure difference then exists between the sample chamber and the standard chamber.
(5) Connect the standard chamber and sample chamber. Methane will now flow from the sample chamber into the standard chamber - increasing the pressure in the standard chamber. During gas production, adjust the measuring pump to maintain the standard chamber at constant pressure. Record volume change in the measuring pump with time until the gas production process is complete.

Based on this time-history of volume change of the measuring pump, evaluate the produced mass via the gas equation of state (Wang et al., 2016a).

2.2. Model assumptions

Gas flow through a porous medium is governed by several factors. These include physical properties of the matrix, patterns of flow and PVT properties of the fluid within the flow system. In order to simplify the mathematical presentation and analysis, the following assumptions are used:

(1) The powdered sample is assumed homogeneous in all properties such as pore structure, permeability and desorption parameters with individual particles assumed spherical;
(2) Single phase spherical flow of gas progresses at constant temperature and boundary pressure. An average permeability is used to depict gas flow in each dynamic gas production stage.
(3) Gas adsorption/desorption capacity is described by a Langmuir isotherm.
(4) It is typical to use the first assumption to simplify mathematical models of gas flow and transport during production (Cui et al., 2009; Fathi and Akkutlu, 2009; Yang et al., 2016; Yuan et al., 2014). Heat liberation (assumption #2) during gas desorption is neglected because the experiment is conducted at prescribed and controlled constant temperature. When temperatures significantly exceed the boiling points of the individual gas species, the thickness of the adsorbed layer decreases and surface diffusion becomes negligible (Darabi et al., 2012; Ruthven, 1984). The assumption of an average permeability or diffusion coefficient within a certain pressure range is accepted and widely used by others (Sang et al., 2016a; Wang et al., 2016b; Yang et al., 2016). Finally, Langmuir isotherms (assumption #3) are broadly applied across this field (Bustin et al., 2008; S. Chen et al., 2017a; Guo et al., 2017, Guo et al., 2013; Ross and Bustin, 2007; Zhai et al., 2014).

2.3. Mathematical model

Before presenting the governing equations in detail, we first discuss some basic concepts for the VPG method.

2.3.1. Effective adsorption porosity

Previous studies indicate that pore size, thickness of the adsorbed gas layer and mean free path of methane are all of nanometer scale (Bustin et al., 2008; Cui et al., 2009; Etminan et al., 2014; Mastalerz et al., 2012; Pang et al., 2016). Porosity and gas flow mechanisms are significantly affected by the occupied layers of adsorbed gas molecules, requiring that this effect is considered in interpreting permeability.

Porosity is reduced when gas is adsorbed to the pore surface. Thus, the effective porosity depends on gas adsorption/desorption properties and experimental pressures, and can be written as (Cui et al., 2009):

$$\phi_e = \phi - (1-\phi)\frac{\partial \rho_{vads}}{\partial \rho} \tag{1}$$

where ϕ_e, is the effective porosity, ϕ, is the porosity obtained from N_2 adsorption, ρ_{vads}, is the adsorbate density per unit sample volume and ρ, is the gas density in void space of the shale samples.

2.3.2. Desorption rate coefficient

Adsorption/desorption characteristics (Chen et al., 2017a; Cui et al., 2009; Ettehadtavakkol and Jamali, 2016; Wang et al., 2016b; Yang et al., 2016; Yuan et al., 2014) are important during gas production from shale. Discrepancy in outcomes may arise if different assumptions and definitions are used when describing the adsorption/desorption process. An instantaneous diffusion–adsorption/desorption (ID) model is established under the hypothesis that the process of adsorption/desorption is independent of pore pressure and immediately reaches equilibrium (Yuan et al., 2014). In the ID model, the Henry's law constant is used to depict the adsorption/desorption characteristics (m^2/m^3). A delayed adsorption–diffusion (DD) model (Wang et al., 2016b; Yang et al., 2016) accommodates gas dissolution processes in the organic matter. In the DD model, flow rates of gas adsorption/desorption on the pore surface and gas diffusion in the pore space are both considered as comparable in magnitude. The units of the adsorption/desorption rate coefficient in the DD model are *1/s*. An alternative desorption rate is defined by the derivative of adsorbate density based on the Langmuir isotherm ($cm^3/(g\,MPa)$) (Chen et al., 2017b).

To avoid confusion over various desorption coefficients, we adopt a dimensionless desorption rate coefficient defined as the derivative of adsorbed gas density to free gas density. This may be defined as:

$$k_{ads} = \frac{\partial \rho_{vads}}{\partial \rho} = \frac{\partial \rho_{vads}/\partial t}{\partial \rho/\partial t} \tag{2}$$

where ρ_{vads}, is adsorbate density per unit sample volume and ρ is gas density in the pore space, which is described with the gas state equation as:

$$\rho = \frac{P}{ZRT} \tag{3}$$

If the adsorbed gas density is proportional to the free gas density, then Henry's law applies and the adsorption rate coefficient k_{ads} is constant. If gas adsorption/desorption isotherms can be approximated by the Langmuir isotherm, the adsorbate density can be written as:

$$\rho_{wads} = \frac{V_L P}{P_L + P} \tag{4}$$

$$\rho_{vads} = \frac{\rho_s \rho_{wads}}{V_{std}} \tag{5}$$

where ρ_{wads}, is adsorbate density per unit sample weight, V_L, is the Langmuir volume. P_L, is the Langmuir pressure, P, is pressure, ρ_s, is density of shale skeleton and V_{std}, is the molar volume of gas at standard pressure and temperature (i.e. 273.15 K and 0.101325 MPa).

A desorption factor f is defined to describe the effect of desorption on gas flow in the pore space, which is written as:

$$f = \frac{1-\phi}{\phi} k_{ads} \tag{6}$$

Substituting Eq. (3) and Eq. (2) into Eq. (1), the effective porosity becomes:

$$\phi_e = \phi(1-f) \tag{7}$$

with the range of desorption factors, f, in the range 0 to 1. When $f = 0$, this corresponds to non-sorbing fluids with $0 < f < 1$ representing sorptive behavior with some delay. When $f = 1$, this is equivalent to the assumption of immediate sorptive equilibrium. The effective porosity becomes zero at $f = 1$, according to Eq. (7), although this may not be the actual condition but is simply used to show identical migration rate between desorption and flow process.

2.3.3. Rarefaction viscosity

Previous studies have demonstrated that the PVT properties of gas in nanoporous media may deviate from those observed in the bulk condition,- referred to as rarefaction or pore-proximity effects (Civan et al., 2011; Islam et al., 2015; Pitakbunkate et al., 2016; Rezaee, 2011; Wang et al., 2018; Zarragoicoechea and Kuz, 2004). This deviation primarily arises from interaction of the gas molecules with the pore wall, and depends on the nanopore diameters in the medium (Didar and Akkutlu, 2013; Rezaee, 2011) in addition to other relevant factors, e.g. pore geometry, wall chemistry and roughness (Eddaoudi et al., 2015; Nguyen et al., 2009). To investigate the behavior of the gas in the shale pores, the compressibility factor of the confined gas is calculated on the basis of bulk fluid formulae (Hall and Yarborough, 1973) by accommodating the critical temperature and pressure relative to the rarefaction effect (Singh and Singh, 2011; Wu et al., 2016). The confined gas viscosity is determined as a function of Knudsen number (Beskok and Karniadakis, 1999) with bulk viscosity determined by empirical

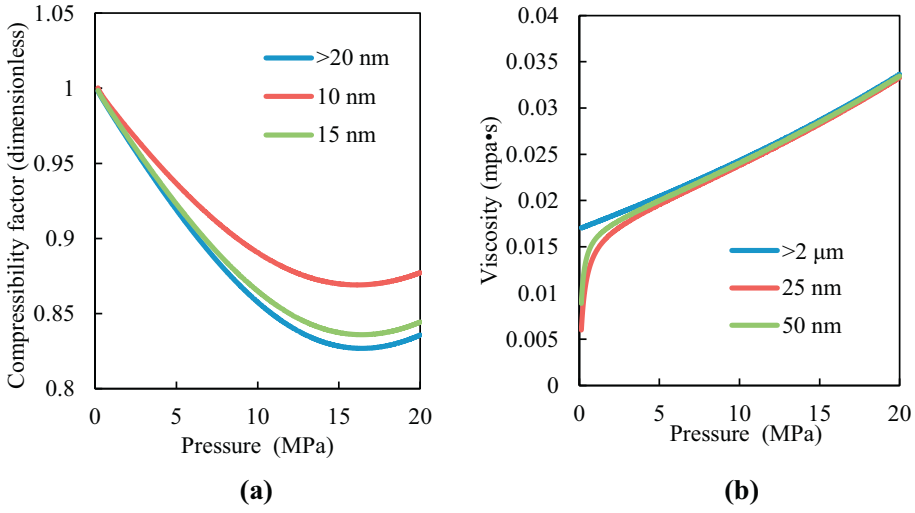

Fig. 3. Methane PVT vs. pressure at 308.15 K. (a) compressibility factor vs. pressure. (b) Viscosity vs. pressure.

formulae (Dempsey, 1965).

Fig. 3 presents the effect of pore size on the confined gas compressibility factor and viscosity. It indicates that the methane compressibility factor is close to its bulk value for pore radii > 20 nm (Fig. 3-a).The confined viscosity clearly deviates from the bulk value for pore radii in the range ~25–50 nm when pressure is lower than ~ 3 MPa (Fig. 3-b). In this study, the average pore sizes in the shale are > 25 nm. Therefore, the effect of rarefaction on the compressibility factor is negligible and Eq. (3) is valid for the calculation. Since the deviation between the confined and the bulk viscosity occurs in the relatively low pressure range considered here, the confined viscosity is modified as:

$$\mu_c = \frac{\mu}{1 + \alpha K_n} \tag{8}$$

where μ_c, is the confined viscosity, μ, is the bulk viscosity, K_n, is the Knudsen number, and α, is a rarefaction coefficient (α = 2) (Michalis et al., 2010).

2.3.4. Pseudo pressure

In the SPG method the analytical equations are solved under the assumption that the gas viscosity, compressibility factor and total porosity are all constant with pressure (Al-Hussainy et al., 1966; Cui et al., 2009; Yang et al., 2015). However these assumptions are inappropriate when measurements are made over a broad pressure range. The governing equation established for real gas flow, considering pressure dependent PVT properties, is nonlinear and complex. In order to linearize the VPG model and account the change of gas PVT properties, a pseudo pressure is defined as (Al-Hussainy et al., 1966):

$$m(P) = 2\int_{P_0}^{P} \frac{P}{\mu_c Z} dP \tag{9}$$

where P_0 is a low base pressure. Eq. (9) is an exact and rigorous transformation of pressure to pseudo-pressure. It follows that:

$$\frac{\partial m(P)}{\partial t} = \frac{\partial m(P)}{\partial p}\cdot\frac{\partial P}{\partial t} = \frac{2P}{\mu_c Z}\cdot\frac{\partial P}{\partial t} \tag{10}$$

and

$$\frac{\partial m(P)}{\partial r} = = \frac{2P}{\mu_c Z}\cdot\frac{\partial P}{\partial r} \tag{11}$$

In order to reduce the error in the numerical integration, the composite trapezoidal rule (Davis and Rabinowitz, 2007) is used to establish the relationship between $m(P)$ and P. The lower limit of the integration P_0 can be set arbitrarily. In this work a value of 0.07 is chosen to establish the relationship between $m(P)$ and P at a temperature of 308.15 K. Sensitivity analyses of the influence of pore size on the $m(P)$-P curve are shown in Fig. 4. This demonstrates that the pore size has negligible effect on the $m(P)$-P curve when the pore radius is greater than ~20 nm.

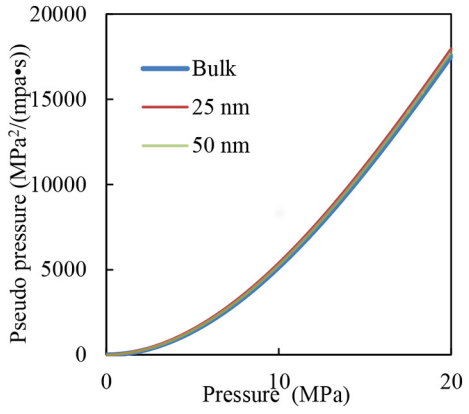

Fig. 4. Relationship between pseudo pressure $m(P)$and pressure P at 308.15 K.

2.3.5. Governing equation

Different from formulating an apparent permeability function to account for the ensemble mechanistic flow mechanisms (e.g. continuous flow, slip flow, Knudsen flow, and others) reported in other studies (Guo et al., 2015; Javadpour et al., 2007; Roy et al., 2003; Singh and Javadpour, 2013), in this work, the permeability is determined by fitting the experimental data and represents the ensemble of all these flow mechanisms (Cui et al., 2009; Darabi et al., 2012; Yang et al., 2016). With the above assumptions and definitions, the material balance equation for dynamic gas desorption-flow in spherical coordinates is:

$$\phi_e\frac{\partial \rho}{\partial t} + (1-\phi_e)k_{ads}\frac{\partial \rho}{\partial t} = \frac{K}{r^2}\frac{\partial}{\partial r}\left(r^2\frac{1}{\mu_c c_g}\frac{\partial \rho}{\partial r}\right) \tag{12-1}$$

where K is the matrix permeability, r is the distance between the point of interest and the center of the spherical model, t is time and c_g is gas compressibility, defined as: $c_g = \frac{1}{P} - \frac{1}{Z}\frac{dZ}{dP}$.

The initial and boundary conditions of the VPG model are:

$$\rho|_{0\le r<R_a, t=0} = \rho_i \tag{12-2}$$

$$\rho|_{r=R_a, t\ge 0} = \rho_0 \tag{12-3}$$

$$\left.\frac{\partial \rho}{\partial r}\right|_{r=0} = 0 \tag{12-4}$$

where R_a is the radius of the particles comprising the bead-pack sample, ρ_i is the initial gas density in the void space of the sample and ρ_0 is the gas density on the external surface of the samples.

Eq. (12) is a non-linear partial differential equation with pressure dependent variables of ϕ_e, k_{ads}, μ_c and c_g. We use the concept of pseudo-pressure to consider the change in the parameters μ and Z. By Substituting Eq. (4), Eq. (9), Eq. (10) and Eq. (11) into Eq. (12), the governing equation for gas flow becomes (*Al*-Hussainy et al., 1966):

$$\phi_e\frac{\partial m(P)}{\partial t} + (1-\phi_e)k_{ads}\frac{\partial m(P)}{\partial t} = \frac{K}{\mu_c c_g}\left(\frac{\partial m(P)}{\partial r^2} + \frac{2}{r}\frac{\partial m(P)}{\partial r}\right) \tag{13-1}$$

$$m(P)|_{0\le r<R_a, t=0} = m_i \tag{13-2}$$

$$m(P)|_{r=R_a, t\ge 0} = m_0 \tag{13-3}$$

$$\left.\frac{\partial m(P)}{\partial r}\right|_{r=0} = 0 \tag{13-4}$$

Eq. (13-1) can be written as:

$$\frac{\partial m(P)}{\partial t} = T_0\left(\frac{\partial m(P)}{\partial r^2} + \frac{2}{r}\frac{\partial m(P)}{\partial r}\right) \tag{14}$$

where

$$T_0 = \frac{K}{\mu_c c_g(\phi_e + (1-\phi_e)k_{ads})} \tag{15}$$

Eq. (14) is a simplified form of Eq. (12) and takes the pressure dependent variables μ_c and Z in to consideration without restriction to small pressure gradients. However, Eq. (14) is still non-linear because T_0 is a function of pressure. Numerical methods can be used to solve the equation with complex manipulation and significant computation (Ettehadtavakkol and Jamali, 2016; Shabro et al., 2012). However, in this paper, we attempt to obtain an approximate solution under reasonable assumptions.

For each gas production stage, the average desorption rate coefficient k_{ads} and effective porosity ϕ_e are used instead of the pressure-dependent variables – this simplifies Eq. (14). After applying the pseudo pressure, the two non-linear variables μ_c and c_g still remain in Eq. (14).

Previous study (Al-Hussainy et al., 1966; Aronofsky and Jenkins, 1954) indicates that for constant rate production from a closed radial system, the real gas pseudo pressure can be correlated as a function of a dimensionless time based on μ_c and c_g evaluated at the initial pressure. This approximation approach is also applicable in our study according to two basic conditions. First, according to the Newman Product method (Gringarten and Ramey, 1973), multi-dimensional flow can be decomposed into several one-dimensional flows, and the solutions of the multi-dimensional flow can be generated by the product of these one-dimensional flow solutions under equivalent boundary conditions. This indicates that the approximation approach can be used in Eq. (14) when the gas production rate is constant. Second, problems of constant pressure and constant production rate can be considered as equivalent, and their solutions can be transformed into each other in Laplace Space (Van-Everdingen and Hurst, 1949). For Eq. (14), the external pressure is constant and the production rate is variable. Therefore, Eq. (14) can be written in a linearized form as:

$$\frac{\partial m_D}{\partial t_D} = T_D\left(\frac{\partial m_D}{\partial r_D^2} + \frac{2}{r_D}\frac{\partial m_D}{\partial r_D}\right) \tag{16-1}$$

$$m_D|_{0\le r_D<1, t_D=0} = 0 \tag{16-2}$$

$$m_D|_{r_D=1, t_D\ge 0} = 1 \tag{16-3}$$

$$\left.\frac{\partial m_D}{\partial r_D}\right|_{r_D=0} = 0 \tag{16-4}$$

with dimensionless formula:

$$T_D = \frac{T_0}{r_w K_m} \tag{17}$$

$$r_D = \frac{r}{R_a} \tag{18}$$

$$t_D = \frac{Kt}{\phi_e \mu_{ci} c_{gi} R_a^2} \tag{19}$$

$$m_D = \frac{m(P) - m(P_i)}{m(P_0) - m(P_i)} \tag{20}$$

where K_m is a mass transfer coefficient characterizing the mass transfer resistance between the external surface of the samples and the void space in the chamber ($K_m = 6 \times 10^{-7}$) (Ettehadtavakkol and Jamali, 2016). Parameters μ_{ci} and c_{gi} are the confined gas viscosity and compressibility under initial conditions, respectively, r_w is the radius of the shale pore, P_0 is the constant external pressure and P_i is the initial gas pressure in the shale sample.

An analytical solution for Eq. (16) can be obtained by Laplace transform (Carslow et al., 1986). The dimensionless pseudo-pressure distribution is given as:

$$m_D = 1 + \sum_{n=1}^{\infty} \frac{2(-1)^n \sin(n\pi r_D) e^{-T_D n^2 \pi^2 t_D}}{n\pi r_D} \tag{21}$$

2.3.6. Permeability determination

The shale matrix production capacity is a function of pressure, which can be defined as:

$$\Omega(\mathrm{P}) = \mathrm{Q}_0 - \left[(1-\phi_e)\frac{V_L P}{P+P_L} + \phi_e \frac{P}{ZRT}\right] \tag{22}$$

where Q_0 is the total gas contained in the shale samples at initial conditions, which can be written as:

$$\mathrm{Q}_0 = \left((1-\phi_e)\frac{V_L P_0}{P_0+P_L} + \phi_e \frac{P_0}{ZRT}\right) \tag{23}$$

We define the fractional production $\mathrm{F_D}$ as the ratio of the cumulative gas production from the shale matrix to the total gas production when the experiment reaches equilibrium pressure $\mathrm{P_0}$:

$$F_D = \frac{\Omega(\overline{\mathrm{P}})}{\mathrm{Q}_0} = 1 - \frac{(1-\phi_e)\frac{V_L \overline{P}}{\overline{P}+P_L} + \phi_e \frac{\overline{P}}{ZRT}}{(1-\phi_e)\frac{V_L P_0}{P_0+P_L} + \phi_e \frac{P_0}{ZRT}} \tag{24}$$

where $\overline{\mathrm{P}}$ is the average pressure throughout the spherical flow mode.

Fig. 4 shows the m(P)-P relation for methane at 308.15 K. The relation is near linear during the primary half of the pressure drop. This means that if the initial pressure is 12 MPa and the external pressure is 6MP, the m(P)-P relation remains linear when the system pressure is larger than 9 MPa. This conclusion is consistent with previous studies (Ettehadtavakkol and Jamali, 2016). If the linear relationship between gas adsorption/desorption capacity ρ_{wads} and pressure P at each substantive production stage holds, then the fractional production can be written as:

$$F_D = 1 - \frac{[(1-\phi_e)k_{ads} + \phi_e]m(\overline{P})}{[(1-\phi_e)k_{ads} + \phi_e]m(P_0)} = 1 - \frac{m(\overline{P})}{m(P_0)} \tag{25}$$

According to Eq. (19), $m_D(P_i) = 0$ is valid. Using this relationship and simple transformation theory, Eq. (25) can be written as:

$$F_D = \frac{m(P_i) - m(\overline{P})}{m(P_i) - m(P_0)} = \overline{m_D}(\mathrm{P}) \tag{26}$$

Where $\overline{m_D}(\mathrm{P})$ is the average dimensionless pseudo pressure defined as:

$$\overline{m_D}(\mathrm{P}) = \int_0^1 m_D(\mathrm{P}) dr_D \tag{27}$$

Substituting Eq. (21) and Eq. (27) in to Eq. (26) we obtain:

$$F_D = 1 + \sum_{n=1}^{\infty} \frac{2(-1)^n sinint(n\pi) e^{-T_D n^2 \pi^2 t_D}}{n\pi} \tag{28}$$

Sinhint (x) in Eq. (28) returns the hyperbolic *sine* integral function of *x* and can be calculated by the *Sinhint* Tool Box in MatLab. Eq. (28) is a general solution describing the relationship between fractional production and time. Permeability and desorption rate coefficient are the only variables with the above assumption during a certain gas dynamic production stage. Those two pareameters can be estimated by nonlinear fitting to match the approximate solution with fractional production data obtained from experiments.

The general solution Eq. (28) contains an infinite term, resulting in difficulties in its evaluation. To accommodate this issue we explore for the sufficient number of terms needed to approximate the general solution. Values of physical parameters are presented as shown in Table 2. Results from Eq. (28) indicate that F_D converges rapidly and can be well approximated using the first 5 terms of the infinite series as shown in Fig. 5. Many similar calculations with different values of basic parameters are performed to confirm this. Thus, Eq. (28) can be approximated as:

Table 2
Basic parameters used establish a relationship between F_D and t.

Property	Unit	Value
Sample radius, R_a	μm	215
Boundary transfer resistance, K_m	μm/s	6e7
Matrix permeability, K	μm^2	7e-9
Initial gas compressibility, c_{gi}	1/Pa	0.911e-7
Initial gas viscosity, μ_{ci}	Pa·s	0.26e-4
Temperature, T	K	308.15
Initial gas pressure, P_i	Pa	15e6
External gas pressure, P_0	Pa	9e6
Skeleton density, ρ_s	g/cm^3	2.73
Shale pore radius, r_w	μm	2e-2
Desorption rate coefficient, k_{ads}	dimensionless	0.0168
Porosity,	ϕ	0.0439

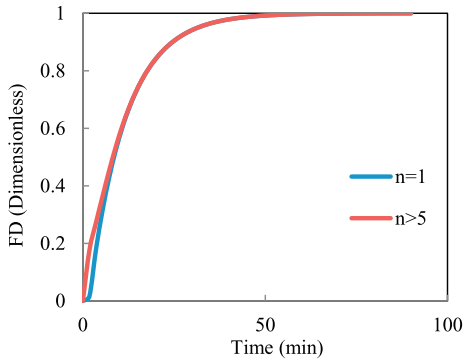

Fig. 5. Convergeing trend for general solution of the VPG model.

$$F_D = 1 + \sum_{n=1}^{5} \frac{2(-1)^{n-1} sinint(n\pi) e^{-T_D n^2 \pi^2 t_D}}{n\pi} \quad (29)$$

Eq. (29) is used to calculate shale matrix permeability by matching the experimental data. The basis of the derivation for Eq. (29) is the linear relationship between pseudo-pressure *m(P)* and actual pressure *P*. This relationship is valid when the value of average pressure in the flow system is larger than the arithmetic mean value between initial pressure and boundary pressure. This corresponds to a transient flow before the pressure drop reaches the pore center. The time for the transient flow is difficult to be accurately estimated in our experiments. In this paper, we first estimate shale permeability and desorption rate coefficient by matching the experimental points of $F_D \leq 0.75$ (Ettehadtavakkol and Jamali, 2016) with Eq. (29) and then generalize to the total number of experimental data points by drawing the F_D-t curves using Eq. (29) with the estimated parameters. This part will be further discussed in Section 3.3.

Through matching the approximate solution in Eq. (29) with the experimental data, permeability estimation is equivalent to an optimization problem to find the minima of the least-squares form (Wang et al., 2016a; Yang et al., 2016). The least-squares form for this specific parameter estimation problem is:

$$Min\ S(\vec{P}) = \frac{1}{2} \sum_{m=1}^{j} (F_{Dcal}(\vec{P}, t_m) - F_{Dexp}(t_m))^2 \quad (30)$$

In Eq. (30), S is the sum of squared residuals, $\vec{P}$ is the vector of estimated parameters and contains desorption rate coefficient and permeability and F_{Dcal} is the calculated gas fractional production from Eq. (29). F_{Dexp} is the experimentally measured gas fractional production, t_m is the time corresponding to the m^{th} experimental point, while j represents the number of experimental points used for the matching process.

The objective function of Eq. (29) is non-linear, which contains multiple local optimum points. To avoid obtaining a local optimal result, rather than the global one, a series of initial values of desorption rate coefficients from 0 to 1 and permeability from 1×10^{-5} md to 1×10^{-8} md are used as the initial value to estimate the shale permeability. A uniformly distributed 10,000 points for desorption rate coefficient and 10,000 points for permeability are generated. Then a fitting algorithm based on the least-squares method is applied to estimate the permeability and desorption coefficient for each initial point (using MatLab). The global optimum solution is obtained by storing the estimated permeability and desorption coefficient corresponding to the minimum *MinS(K)*.

3. Results and discussion

This section first presents the results of static and dynamic experiments for samples of three different particle sizes at three different pressure gradients. Then shale matrix permeability is determined by fitting the experimental results. Effects of pore pressure and particle size on the resulting permeability are investigated. Finally, the SPG and VPG methods are analyzed and discussed.

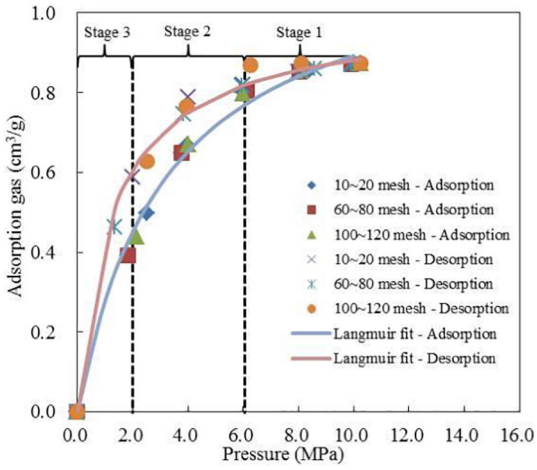

Fig. 6. Experimental and Langmuir fitting adsorption/desorption results for three different particle sizes with the desorption isotherm divided into three stages by the dash line.

3.1. Methane static adsorption/desorption

Results from methane adsorption/desorption experiments for three different particle sizes at a temperature of 308.15 K are shown in Fig. 6. Both the experimental data and Langmuir fitting curves are presented. It indicates that particle size negligibly affects the evaluated adsorption/desorption isotherms. This result is consistent with that of previous studies (Wang et al., 2016a; Yang et al., 2016; Yuan et al., 2014). The desorption isotherm exceeds the adsorption isotherm, indicating hysteresis during desorption. This phenomenon can be explained by the variation of pore throat size (Chen et al., 2017a) during desorption. A Langmuir model can be used to match the experimental data. The Langmuir pressure P_L and Langmuir volume V_L for adsorption and desorption isotherms are 3.246 MPa, 1.182 m^3/g, and 1.315 MPa, 0.998 m^3/g, respectively.

The Langmuir desorption isotherm of Fig. 6 also indicates that the gas desorption process can be divided into several stages. Prior studies (Chen et al., 2017b) have demonstrated that the desorption process is divided into three stages - according to the change rate of gas adsorption capacity per incremented pressure drop. The derivative of the static Langmuir model is used to analyze the change of desorption rate with pressure. However, the gas desorption process is a dynamic process. The use of a static model may lead to erroneous conclusions. In this paper, the gas desorption process is also divided into three stages with individual pressure ranges of 0–2 MPa, 2–6 MPa and 6–10 MPa according to the approach (Chen et al., 2017b) shown in Fig. 6. Dynamic gas production tests are conducted with those three different pressure drops as the production characteristics presented in the next section.

3.2. Methane dynamic production

The results for gas production experiments with three different pressure ranges for three samples of different particle sizes (i.e. 10–20 mesh, 60–80 mesh and 100–120 mesh) at 308.15 K are shown versus time in Fig. 7. For each gas production stage, gas accumulative production is almost the same for different particle sizes. There are two reasons accounting for this phenomenon. One is that the specific surface area of micro and macro pores in shale is several times greater than the bulk surface area – thus making the effect of particle size on the adsorption area negligible. Another reason is that the pressure drop and

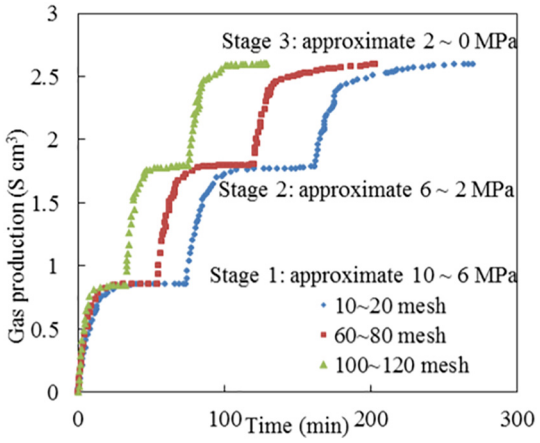

Fig. 7. Gas dynamic production with different pressure drops for three particle sizes.

pore volume are almost the same for each particle size, suggesting that the same free gas amount is produced from the pores. Therefore the same gas accumulative production applies to particles of different sizes at each production stage. Fig. 7 also shows that the larger the particle size, the greater the time taken to reach equilibrium. i.e., the total equilibration times are 73 min, 54 min and 32 min for particle sizes range from large to small over the first stage. The two experimental results above are consistent with many previous studies (Wang et al., 2016a; Yang et al., 2016; Yuan et al., 2014).

After conducting the dynamic gas production experiments noted above, fractional production F_D data of real gas production can be straightforwardly obtained and used to determine the permeability and desorption rate coefficient. Eq. (29) is used to determine the flow parameters based on the MatLab program presented in Section 2.3.5 by matching the experimental data for $F_D < 0.75$. Then the fractional production F_D data for the other part is calculated. Fig. 8 presents the fitting curves for the experimental results with three particle sizes at each dynamic production stage. From Fig. 8, it is clear that the calculated F_D from the mathematical model matches the experimental data for the entire process of the first and the second production stages. However, the model deviates from the experimental results in the third production stage when $F_D > 0.75$.

In order to estimate the accuracy of the calculated results for each production stage, the average absolute error (AAE) and average absolute relative error (AARE) are used to describe the difference between experimental and calculated values of F_D. These are defined as:

$$\mathrm{AAE} = \frac{1}{N}\sum_{i=1}^{N} |F_{D,i}^{exp} - F_{D,i}^{cal}| \tag{31}$$

$$\mathrm{AARE} = \frac{1}{N}\sum_{i=1}^{N} \left|\frac{F_{D,i}^{exp} - F_{D,i}^{cal}}{F_{D,i}^{exp}}\right| \tag{32}$$

where $F_{D,i}^{exp}$ and $F_{D,i}^{cal}$ are the ith fractional production obtained from experiment and the VPG model and where N are the total number of experimental points.

The standardized residual SR is used to identify outliers an individual datum that may differ from the bulk of the data present in a dataset (Feng et al., 2014), which is defined as:

$$\mathrm{SR} = \frac{F_{D,i}^{exp} - F_{D,i}^{cal}}{F_{D,i}^{exp}\, SD} \tag{33}$$

where SD is the standard deviation of the difference between F_D obtained from experiment and that from the VPG model. This may be written as:

$$\mathrm{SD} = \sqrt{\frac{\sum_{i=1}^{N}\left(\frac{F_{D,i}^{exp} - F_{D,i}^{cal}}{F_{D,i}^{exp}}\right)^2}{N-1}} \tag{34}$$

Table 3 shows the estimated parameters and errors at each production stage for three particle sizes. The effects of particle size and pressure drop on permeability will be discussed in the following section. In this section, we focus on analyzing the errors of the VPG model. As is shown, the AAE and AARE for the first and second production stages are estimated to be < 0.0401 and 5.88%, respectively. Considering the uncertainties in measuring gas dynamic production curves, it is suggested that the errors arising in the VPG estimations are within an acceptable range for the first and second production stages. The AAE and AARE for the third production stage are up to 0.0944 and 16.68% respectively, which may exceed a desired acceptance range. This is consistent with the result of the obvious difference between the measured and calculated F_D shown in Fig. 8. However, the derivation of the calculated F_D from the measured F_D evidently only occurs when the values of F_D are larger than 0.75, where the gas production has approached full recovery. Therefore the obvious difference between the measured and calculated F_D may not play a significant effect on the evaluation of gas production. The standardized residual plots of the third production stage for the three particle sizes may offer support for this argument. Fig. 9 presents the distribution of standardized residuals along with the measured F_D, where only 3 out of 103 data points fall outside the $[-2, +2]$ range and are identified to be outliers. In general, when the model is correct, the standardized residuals tend to fall in the range $[-2, +2]$ and are randomly distributed with a zero mean (Feng et al., 2014). Therefore, the VPG model is still valid when applied to the third production stage.

3.3. Effect of pore pressure

During the dynamic production process for a certain pressure drop, a typical pressure distribution in a spherical shale particle is as depicted in Fig. 10. At the beginning of the gas production process, the external pressure is suddenly dropped from the initial pressure P_i to a lower pressure P_0. Both free gas flow (a combination of several flow mechanisms involving continuous flow, slip flow and Knudsen flow) and adsorbed gas desorption progress with gas production from the pore and develop a pressure gradient as the external surface is approached. As time elapses and gas is produced, the pressure drop migrates to the interior of the particle. The transient stage defined as the gas production process before the pressure drop reaches the particle center. When the pressure drop reaches the center of the particle, the gas production process evolves to boundary dominated flow. Eventually, a uniform pressure distribution inside the cylindrical pore is attained and the gas production process terminates.

Two parameters are used to characterize the dynamic production behavior - the permeability to free gas flow in a cylindrical pore and the desorption rate coefficient for gas desorption into the pore space. Since an interplay between the free gas flow and the adsorbed gas desorption exists in the gas production process, it is difficult to determine the two flow parameters, separately. Therefore, permeability is estimated simultaneously with desorption rate coefficient by using Eq. (29) to match the experimental data. The results at different initial pressure drops are shown in Table 3. As presented, the gas permeability is of the order magnitude of 10^{-7}–10^{-6} md and decreases with a decrease in the average pore pressure. Considering gas production in shale with an average diameter of 1265 μm as an example - when the external pressure decreases from 5.92 to 0.14 MPa (average pore pressure decreases from 7.93 to 1.19 MPa) the gas permeability decreases from

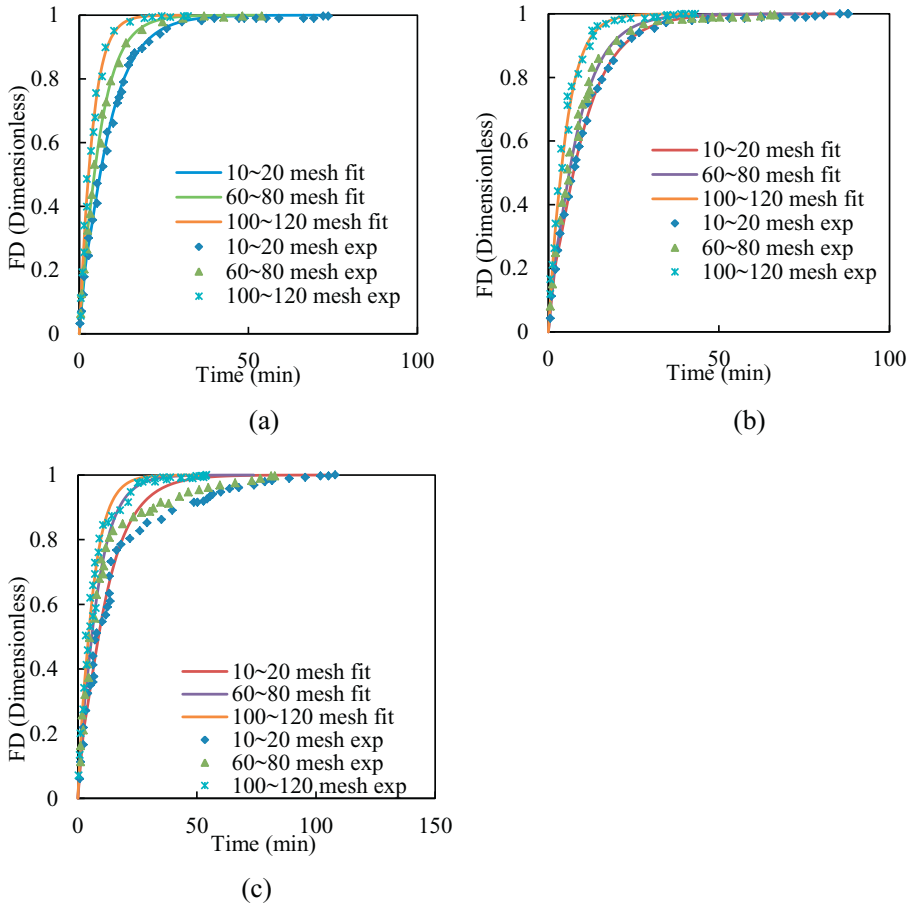

Fig. 8. F_D vs. time curves for both mathematical model fitting and experimental results. (a), (b) and (c) represent three gas dynamic production stages with pressure drops approximately from 10 to 6 MPa, from 6 to 2 MPa and from 2 to 0 MPa, respectively.

Table 3
Estimated parameters and errors for each production stage.

Average diameter, (μm)	Pressure step, (MPa)	Permeability, (10^{-7}md)	Desorption rate 10^{-3}	AAE (Dimensionless)	AARE (%)
1265	9.94–5.92	25.1	5.42	0.0171	4.94
	5.92–2.03	23.2	4.75	0.0109	5.88
	2.03–0.14	20.3	3.93	0.0385	7.84
215	9.98–5.96	4.68	4.23	0.0287	4.47
	5.96–1.98	4.02	3.65	0.0401	7.41
	1.98–0.13	3.33	2.61	0.0944	16.68
135	9.97–6.01	4.05	4.07	0.0174	3.55
	6.01–2.01	3.53	3.38	0.0186	4.06
	2.01–0.14	3.10	2.46	0.0251	4.89

25.1×10^{-7} md to 21.5×10^{-7} md.

From Table 3, it is apparent that the desorption rate coefficient is of the order of magnitude of 10^{-3}. According to Eq. (6), the desorption factor f is calculated to be much smaller than 1, such that the desorption process is delayed in the gas recovery from a cylindrical pore.

Table 3 also indicates that the desorption rate coefficient decreases with the decrease of average pore pressure. This leads to a smaller value of permeability at relatively low average pore pressure. At relatively low pore pressure, the mean free path of gas molecules may be much greater than the pore width and slip flow may occur (Heller et al., 2014). This offers a transport mechanism to accelerate the gas flow. The smaller permeability at relatively low pressure indicates that the gas flow is much more sensitive to decreases in desorption rate than increases in gas flow rate caused by slip flow. Therefore, the permeability change observed for methane is different from that measured for helium. This is well known, since helium is a non-sorbing gas and its flow rate is only affected by the flow regime.

3.4. Effect of particle size

According to Table 3, the permeability decreases when gas production tests are conducted on smaller particle sizes. Considering gas production with a pressure drop from ~10 to 6 MPa as an example, the permeability is 25.1×10^{-7}, 4.68×10^{-7} and 4.05×10^{-7} md for

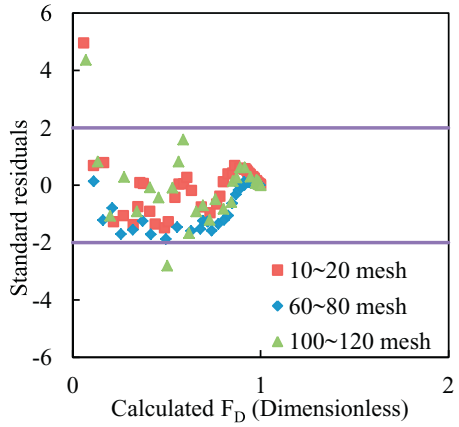

Fig. 9. Calculated standardized residuals vs. measured F_D.

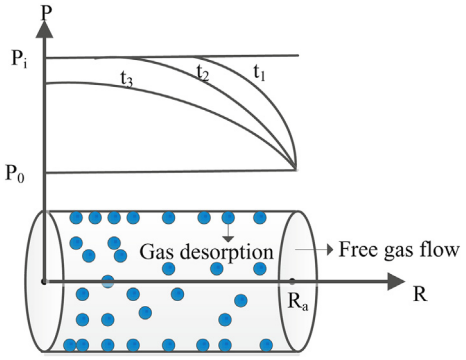

Fig. 10. Typical pressure distribution in a cylindrical pore of a spherical shale particle.

particle sizes of 1265 μm, 215 μm and 135 μm, respectively. This phenomenon is not caused by changes of physical properties of the gas and flow regimes, because the gas properties and flow regimes are essentially constant within the same pressure drop. The most probable reason for the decrease in the true magnitude of the permeability with the decrease in particle size – that is that large pores may be damaged when the sample is crushed to smaller fractions. The disappearance of some large pores may result in smaller pore channels, which may in turn lead to lower permeability in smaller particle sizes. This conclusion is consistent with previous results that the measured permeability of shale cores that are much larger than those of powdered shale particles (Cui et al., 2009; Heller et al., 2014; Yang et al., 2016).

3.5. Model comparison and analysis

The main difference between the traditional small pressure gradient (SPG) method and the VPG method is that the physical parameters of the gas are all considered to be constant under an average pressure in the SPG method. When the VPG method is conducted with a small pressure gradient, the assumption of constant gas PVT parameters remains valid. In other words, the VPG model simplifies into the SPG model under the same boundary conditions. Permeability determined from the SPG method can only depict gas flow at a certain average pressure. In order to describe gas flow over a large pressure gradient, the geometric or arithmetic mean between permeability at initial pressure and that at equilibrium pressure measured by SPG are calculated to describe the gas flow behavior. However, previous studies (Cui and Abass, 2016) indicate that permeability of tight formations is not a monotonic function of the average reservoir pressure. When the pore pressure is lower than a critical pressure, increasing the pore pressure will lead to a smooth and linear increase in permeability. When the critical pore pressure is exceeded, the change of permeability will transition from a linear to an exponential increase with the increase in pore pressure. Therefore, it is inaccurate to determine permeability using the SPG method when gas is produced with large pressure gradients.

Conversely, the VPG method is a straightforward approach to obtain permeability under multiple pressure gradient conditions. The disadvantages of the VPG method presented in this paper include potentially eliminating the effects of moisture and the inability to measure how permeability evolves under different confining pressures. To rectify this shortcoming, the dynamic gas production test method should be applied to powdered samples saturated with in situ moisture conditions and under appropriate confining pressures.

4. Conclusions

Shale matrix permeability is a critical parameter controlling long-term gas production requiring reliable measurement to appropriately evaluate the reserve potential of reservoirs. However, current methods using nitrogen or helium to measure the permeability with small pressure gradients are insufficient due to the impacts of strong adsorption/desorption effects for real gases and distinct changes of gas PVT properties. Using methane to measure permeability with a variable pressure gradient is therefore preferred, requiring that desorption processes and real PVT characteristics are considered. A VPG method is presented to determine shale matrix permeability using methane by coupling a mathematical model with dynamic gas production data. Dynamic gas production experiments under constant boundary pressures are conducted in powdered particles of three different sizes at 308.15 K. A mathematical model is established by accommodating desorption processes and the effect of variations of pressure-dependent viscosity and compressibility. The permeability and desorption rate coefficient are determined by matching the approximate solutions with the experimentally determined gas production data. The major conclusions are:

(1) Approximate solution of the mathematical model is obtained based on the linear relationship between adsorption gas density ρ_{wads} and pseudo pressure $m(p)$. When the fractional production F_D is < 0.75, the calculated F_D fits the experimental results well at any average pore pressure condition. When F_D exceeds 0.75, differences may occur between the calculated and measured F_D. Since the differences appear when the gas recovery approaches completion, those predicted deviations can be accepted during gas production in real reservoirs.
(2) The gas permeability obtained in these evaluations is of the magnitude of 10^{-7}–10^{-6} md. The permeability will decrease with a decrease in the average pore pressure for particle sizes used in our experiments.
(3) The desorption process has a delayed effect on gas flow in the cylindrical pores. When the average pore pressure decreases, gas flow is much more sensitive to decreases in desorption rate than increases in gas flow rate caused by slip flow.
(4) The VPG method is a straightforward approach to obtain permeability under multiple pressure gradient conditions. Although effects of moisture and effective pressure are not considered in the VPG model, related studies may be readily conducted, based on the approach presented in the VPG method.

Acknowledgments

The authors are grateful for the important support from 973 project (2014CB239103), the National Science, Technology Major Project (2016ZX05023-001, 2017ZX05049-006) and the Fundamental Research Funds for Central Universities (No. 15CX06026A) the China Scholarship Council (No. 201706450021), the Graduate Innovation

Fund Project of China University of Petroleum (Huadong) (No. YCXJ2016018).

Nomenclature

ϕ_e	Effective porosity of the shale samples, dimensionless
ϕ	Porosity of shale samples, dimensionless
ρ_{vads}	Adsorbate density per unit sample volume, mol/m^3
ρ	Gas density in void space of the shale samples, mol/m^3
f	Desorption factor, dimensionless
ρ_i	Initial gas density in void space of the shale samples, mol/m^3
ρ_0	Gas density in the external surface of the shale samples, mol/m^3
P_i	Initial gas pressure in sample chamber, Pa
P_0	Gas pressure in the external surface, Pa
ρ_{wads}	Adsorbate density per unit sample weight, cm^3/gh
V_L	Langmuir volume, cm^3/g
P_L	Langmuir pressure, Pa
P	Pressure, Pa
P_0	Constant external pressure, Pa
P_i	Initial gas pressure in shale sample, Pa
ρ_s	Density of shale skeleton, g/cm^3
V_{std}	Molar volume of gas at standard pressure and temperature (i.e. 273.15 K and 0.101325 MPa) 22.413 × 10^{-3} m^3/mol
Z	Gas compressibility factor, dimensionless
R	Universal constant, 8.314 J/(K mol)
T	Temperature, K
c_g	Gas compressibility, 1/Pa
c_{gi}	Gas compressibility in initial conditions, 1/Pa
k_{ads}	Desorption rate coefficient, dimensionless
K	Matrix permeability, μm^2
K_m	Boundary transfer resistant, μm/s
r	Distance between analyzed point and the center of the spherical model, μm
t	Time, s
R_a	Radius of shale samples, μm
T_0	Diffusivity coefficient, μm^2/s
μ	Gas viscosity, Pa·s
μ_c	Confined gas viscosity, Pa·s
μ_{ci}	Confined gas gas viscosity in initial conditions, Pa·s
r_w	Radius of shale pore, μm
$m(P)$	Pseudo-pressure, Pa/s
Q_0	Total gas contained in shale samples before gas production, cm^3/g
T_D	Dimensionless diffusivity coefficient
m_D	Dimensionless pseudo pressure
r_D	Dimensionless distance
t_D	Dimensionless time
F_D	Fractional production, dimensionless
Ω(P)	Shale matrix production capacity at pressure P, cm^3/g.
$F_{D,\ i}{}^{exp}$	The ith fractional production obtained from experiment, dimensionless
$F_{D,\ i}{}^{cal}$	The ith fractional production obtained from the VPG model, dimensionless

References

Al-Hussainy, R., Ramey, H.J., Crawford, P.B., 1966. The flow of real gases through porous media. J. Pet. Technol. 18, 624–636.

API, 1998. Recommended Practices for Core Analysis. http://w3.energistics.org/RP40/rp40.pdf.

Aronofsky, J.S., Jenkins, R., 1954. A simplified analysis of unsteady radial gas flow. J. Pet. Technol. 6, 23–28.

Azom, P.N., Javadpour, F., 2012. Dual-continuum modeling of shale and tight gas reservoirs. In: SPE Annual Technical Conference and Exhibition. October, San Antonio, Texas, USA, pp. 8–10.

Barrett, E.P., Joyner, L.G., Halenda, P.P., 1951. The determination of pore volume and area distributions in porous substances I. Computations from Nitrogen Isotherms. J. Am. Chem. Soc. 73, 373–380.

Bernabé, Y., Mok, U., Evans, B., 2006. A note on the oscillating flow method for measuring rock permeability. Int. J. Rock Mech. Min. Sci. 43, 311–316.

Beskok, A., Karniadakis, G.E., 1999. Report: a model for flows in channels, pipes, and ducts at micro and nano scales. Microscale Thermophys. Eng. 3, 43–77.

Bourbie, T., Walls, J., 1982. Pulse decay permeability: analytical solution and experimental test. Soc. Pet. Eng. J. 22, 719–721.

Brace, W.F., Walsh, J.B., Frangos, W.T., 1968. Permeability of granite under high pressure. J. Geophys. Res. 73, 2225–2236.

Brunauer, S., Emmett, P.H., Teller, E., 1938. Adsorption of gases in multimolecular layers. J. Am. Chem. Soc. 60, 309–319.

Bustin, A.M.M., Bustin, R.M., 2012. Importance of rock properties on the producibility of gas shales. Int. J. Coal Geol. 103, 132–147.

Bustin, R.M., Bustin, A.M.M., Cui, A., Ross, D., Pathi, V.M., 2008. Impact of shale properties on pore structure and storage characteristics. In: SPE Shale Gas Production Conference. November, Fort Worth, Texas, USA, pp. 16–18.

Carlson, E., Mercer, J., 1991. Devonian shale gas production: mechanisms and simple models. J. Pet. Technol. 43, 476–482.

Carslow, H.S., Jaeger, J.C., Morral, J.E., 1986. Conduction of Heat in Solids, second ed. The Flow of Heat in A Sphere and Core. Clarendon, New York, pp. 231–233.

Chen, S., Qin, Y., Zhang, Q., Du, L., Zhao, J., 2017b. Numerical description of shale gas desorption stages. Energy Explor. Exploit. 35, 734–747.

Chen, J., Wang, F.C., Liu, H., Wu, H.A., 2017a. Molecular mechanism of adsorption/desorption hysteresis: dynamics of shale gas in nanopores. Sci. China Phys. Mech. Astron. 60, 1–8.

Chen, S., Zhu, Y., Wang, H., Liu, H., Wei, W., Fang, J., 2011. Shale gas reservoir characterisation: a typical case in the southern Sichuan Basin of China. Energy 36, 6609–6616.

Civan, F., Rai, C.S., Sondergeld, C.H., 2011. Shale-gas permeability and diffusivity inferred by improved formulation of relevant retention and transport mechanisms. Transp. Porous Media 86, 925–944.

Clarkson, C.R., Solano, N., Bustin, R.M., Bustin, A.M.M., Chalmers, G.R.L., He, L., Melnichenko, Y.B., Radliński, A.P., Blach, T.P., 2013. Pore structure characterization of North American shale gas reservoirs using USANS/SANS, gas adsorption, and mercury intrusion. Fuel 103, 606–616.

Cui, Q., Abass, H.H., 2016. Experimental study of permeability decline in tight formations during long-term depletion. In: SPE Low Perm Symp, 5–6 May, Denver, Colorado, USA.

Cui, X., Bustin, A.M.M., Bustin, R.M., 2009. Measurements of gas permeability and diffusivity of tight reservoir rocks: different approaches and their applications. Geofluids 9, 208–223.

Darabi, H., Ettehad, A., Javadpour, F., Sepehrnoori, K., 2012. Gas flow in ultra-tight shale strata. J. Fluid Mech. 710, 641–658.

Davis, P.J., Rabinowitz, P., 2007. Methods of Numerical Integration. Acdamic, New York.

Dempsey, J.R., 1965. Computer routine treats gas viscosity as a variable. Oil Gas J. 63, 141–143.

Dicker, A.I., Smits, R.M., 1988. A practical approach for determining permeability from laboratory pressure-pulse decay measurements. In: International Meeting on Petroleum Engineering. November, Tianjin, China, pp. 1–4.

Didar, B.R., Akkutlu, I.Y., 2013. Pore-size dependence of fluid phase behavior and properties in organic-rich shale reservoirs. In: SPE International Symposium on Oilfield Chemistry. April, Woodlands, Texas, USA, pp. 8–10.

Ding, W., Li, C., Li, C., Xu, C., Jiu, K., Zeng, W., Wu, L., 2012. Fracture development in shale and its relationship to gas accumulation. Geosci. Front. 3, 97–105.

Dubost, F.X., 2012. Production forecasting for shale gas exploration prospects based on statistical analysis and reservoir simulation. In: SPE Latin America and Caribbean Petroleum Engineering Conference. April, Mexico City, Mexico, pp. 16–18.

Eddaoudi, M., Sava, D.F., Eubank, J.F., Adil, K., Guillerm, V., 2015. Zeolite-like metal–organic frameworks (ZMOFs): design, synthesis, and properties. Chem. Soc. Rev. 44, 228–249.

Egermann, P., Lenormand, R., Longeron, D., Zarcone, C., 2002. A fast and direct method of permeability measurements on drill cuttings. In: SPE Annual Technical Conference and Exhibition, 29 September-2 October, San Antonio, Texas.

Etminan, S.R., Javadpour, F., Maini, B.B., Chen, Z., 2014. Measurement of gas storage processes in shale and of the molecular diffusion coefficient in kerogen. Int. J. Coal Geol. 123, 10–19.

Ettehadtavakkol, A., Jamali, A., 2016. Measurement of shale matrix permeability and adsorption with canister desorption test. Transp. Porous Media 114, 149–167.

Fathi, E., Akkutlu, I.Y., 2009. Matrix heterogeneity effects on gas transport and adsorption in coalbed and shale gas reservoirs. Transp. Porous Media 80, 281–304.

Fathi, E., Tinni, A., Akkutlu, I.Y., 2012. Shale gas correctiton to klinkenberrg slip theory. In: SPE Americas Unconventional Resources Conference, Pittsburgh, Pennsylvania, USA.

Feng, Q., Zhang, J., Zhang, X., Shu, C., Wen, S., Wang, S., Li, J., 2014. The use of alternating conditional expectation to predict methane sorption capacity on coal. Int. J. Coal Geol. 121, 137–147.

Fischer, G.J., 1992. Chapter 8 the determination of permeability and storage capacity: pore pressure oscillation method. Int. Geophys. 51, 187–211.

Fraim, M.L., Wattenbarger, R.A., 1987. Gas reservoir decline-curve analysis using type curves with real gas Pseudopressure and normalized time. SPE Form. Eval. 2, 671–682.

Freeman, C.M., Moridis, G.J., Blasingame, T.A., 2011. A numerical study of microscale flow behavior in tight gas and shale gas reservoir systems. Transp. Porous Media 90, 253–268.

Gasparik, M., Ghanizadeh, A., Bertier, P., Gensterblum, Y., Bouw, S., Krooss, B.M., 2012. High-Pressure Methane Sorption Isotherms of Black Shales from The Netherlands.

Energy Fuel 26, 4995–5004.
Gringarten, A.C., Ramey, J.H.J., 1973. The use of source and Green's functions in solving unsteady-flow problems in reservoirs. SPE J. 13, 285–296.
Groen, J.C., Peffer, L.A.A., Pérez-Ramírez, J., 2003. Pore size determination in modified micro- and mesoporous materials. Pitfalls and limitations in gas adsorption data analysis. Microporous Mesoporous Mater. 60, 1–17.
Guo, W., Hu, Z., Zhang, X., Yu, R., Wang, L., 2017. Shale gas adsorption and desorption characteristics and its effects on shale permeability. Energy Explor. Exploit. 35, 463–481.
Guo, W., Xiong, W., Gao, S., Zhiming, H.U., Liu, H., Rongze, Y.U., 2013. Impact of temperature on the isothermal adsorption/desorption of shale gas. Pet. Explor. Dev. 40, 514–519.
Guo, C., Xu, J., Wu, K., Wei, M., Liu, S., 2015. Study on gas flow through nano pores of shale gas reservoirs. Fuel 143, 107–117.
Hall, K.R., Yarborough, L., 1973. A new equation of state for Z-factor calculations. Oil Gas J. 71, 82–92.
Handwerger, D. a, Suarez-Rivera, R., Vaughn, K.I., Keller, J., 2011. Improved Petrophysical Core Measurements on Tight Shale Reservoirs Using Retort and Crushed Samples. In: SPE Annual Technical Conference and Exhibition, 30 October-2 November, Denver, Colorado, USA.
Hartwig, A., Könitzer, S., Schulz, H., Horsfield, B., 2009. Investigations of the shale gas potential in NE Germany. In: EGU General Assembly. April, Vienna, Austria, pp. 19–24.
Heller, R., Vermylen, J., Zoback, M., 2014. Experimental investigation of matrix permeability of gas shales. Am. Assoc. Pet. Geol. Bull. 98, 975–995.
Hsieh, P.A., Tracy, J.V., Neuzil, C.E., Bredehoeft, J.D., Silliman, S.E., 1981. A transient laboratory method for determining the hydraulic properties of “tight” rocks-I. Theory. Int. J. Rock Mech. Min. Sci. 18, 245–252.
Islam, A.W., Patzek, T.W., Sun, A.Y., 2015. Thermodynamics phase changes of nanopore fluids. J. Nat. Gas Sci. Eng. 25, 134–139.
Javadpour, F., 2009. Nanopores and apparent permeability of gas flow in mudrocks (shales and siltstone). J. Can. Pet. Technol. 48, 16–21.
Javadpour, F., Fisher, D., Unsworth, M., 2007. Nanoscale gas flow in shale gas sediments. J. Can. Pet. Technol. 46, 55–61.
Jones, S.C., 1972. A rapid accurate unsteady-state Klinkenberg permeameter. Soc. Pet. Eng. J. 12, 383–397.
Kazemi, M., Borujeni, A.T., 2015. Predicting gas apparent permeability of shale samples: a novel analytical approach. In: SPE Annual Technical Conference and Exhibition. September, Houston, Texas, USA, pp. 28–30.
Klinkenberg, L.J., 1941. The permeabiliity of porous media to liquids and gases. In: API Drilling and Production Practice, 1 January, New York, USA.
Li, T., Wu, C., 2015. Research on the abnormal isothermal adsorption of shale. Energy Fuel 29, 634–640.
Lin, W., 1977. Compressibility Fluid Flow through Rocks of Variable Permeability. Lawrence Radiat. https://www.osti.gov/servlets/purl/7080925.
Luffel, D.L., Hopkins, C.W., Schettler, P.D., 1993. Matrix permeability measurement of gas productive shales. In: SPE Annual Technical Conference and Exhibition. October, Houston, Texas, USA, pp. 3–6.
Mastalerz, M., He, L., Melnichenko, Y.B., Rupp, J.A., 2012. Porosity of coal and shale: insights from gas adsorption and SANS/USANS techniques. Energy Fuel 26, 5109–5120.
Michalis, V.K., Kalarakis, A.N., Skouras, E.D., Burganos, V.N., 2010. Rarefaction effects on gas viscosity in the Knudsen transition regime. Microfluid. Nanofluid. 9, 847–853.
Milner, M., McLin, R., Petriello, J., 2010. Imaging texture and porosity in mudstones and shales: comparison of secondary and ion-milled Backscatter SEM methods. In: Canadian Unconventional Resources and International Petroleum Conference. October, Calgary, Alberta, Canada, pp. 19–21.
Neuzil, C.E., Cooley, C., Silliman, S.E., Bredehoeft, J.D., Hsieh, P.A., 1981. A transient laboratory method for determining the hydraulic properties of “tight” rocks-II. Application. Int. J. Rock Mech. Min. Sci. 18, 253–258.
Nguyen, T.X., Bae, J.S., Wang, Y., Bhatia, S.K., 2009. On the strength of the hydrogen-carbon interaction as deduced from physisorption. Langmuir 25, 4314–4319.
Okamoto, N., Liang, Y., Murata, S., Matsuoka, T., Akai, T., Takagi, S., 2015. Slip velocity and permeability of gas flow in nanopores for shale gas. In: SPE Asia Pacific Unconventional Resources Conference and Exhibition. November, Brisbane, Australia, pp. 9–11.
Ozkan, E., Raghavan, R., Petroleum, P., Retd, C., Apaydin, O.G., 2010. Modeling of fluid transfer from shale matrix to fracture network. In: SPE Annual Technical Conference and Exhibition. September, Florence, Italy, pp. 19–22.
Pang, Y., Soliman, M.Y., Deng, H., Emadi, H., 2016. Effect of methane adsorption on stress-dependent porosity and permeability in shale gas reservoirs. In: SPE Low Perm Symposium, 5–6 May, Denver, Colorado, USA.
Pitakbunkate, T., Balbuena, P.B., Moridis, G.J., Blasingame, T.A., 2016. Effect of confinement on pressure/volume/temperature properties of hydrocarbons in shale. Soc. Pet. Eng. J. 21, 621–634.
Qu, H., Zhou, F., Xue, Y., Key, S., Resources, P., 2015. Experimental study of controlling factors of the continental shale matrix permeability in ordos basin geologic characterization of the yanchang formation. In: SPE Asia Pacific Unconventional Resources Conference and Exhibition. November, Brisbane, Australia, pp. 9–11.
Rexer, T.F.T., Benham, M.J., Aplin, A.C., Thomas, K.M., 2013. Methane adsorption on shale under simulated geological temperature and pressure conditions. Energy Fuel 27, 3099–3109.
Rezaee, R., 2011. Fundamentals of gas shale reservoirs, characterization of fluid behavior and equations of state valid for nanoporous media. John Wiley & Sons, New Jersey, pp. 275–277.
Ross, D.J.K., Bustin, R.M., 2007. Impact of mass balance calculations on adsorption capacities in microporous shale gas reservoirs. Fuel 86, 2696–2706.
Ross, D.J.K., Bustin, R.M., Zhang, T., Ellis, G.S., Ruppel, S.C., Milliken, K., Yang, R., 2012. Effect of organic-matter type and thermal maturity on methane adsorption in shale-gas systems. Org. Geochem. 47, 120–131.
Roy, S., Raju, R., Chuang, H.F., Cruden, B.A., Meyyappan, M., 2003. Modeling gas flow through microchannels and nanopores. J. Appl. Phys. 93, 4870–4879.
Ruthven, D.M., 1984. Principles of Adsorption and Adsorption Processes. Wiley, New York.
Sakhaee-Pour, A., Bryant, S.L., 2011. Gas permeability of shale. In: SPE Annual Technical Conference and Exhibition, 30 October-2 November. USA, Denver, Colorado.
Sang, Q., Li, Y., Yang, Z., Zhu, C., Yao, J., Dong, M., 2016a. Experimental investigation of gas production processes in shale. Int. J. Coal Geol. 159, 30–47.
Sang, Q., Li, Y., Zhu, C., Zhang, S., Dong, M., 2016b. Experimental investigation of shale gas production with different pressure depletion schemes. Fuel 186, 293–304.
Shabro, V., Torres-Verdín, C., Javadpour, F., Sepehrnoori, K., 2012. Finite-difference approximation for fluid-flow simulation and calculation of permeability in porous media. Transp. Porous Media 94, 775–793.
Singh, H., Javadpour, F., 2013. A new non-empirical approach to model transport of fluids in shale gas reservoirs. In: SPE Unconventional Resources Conference. August, Calgary, Alberta, Canada, pp. 12–14.
Singh, H., Javadpour, F., Ettehadtavakkol, A., Darabi, H., 2014. Nonempirical apparent permeability of shale. SPE Reserv. Eval. Eng. 17, 414–424.
Singh, S.K., Singh, J.K., 2011. Effect of pore morphology on vapor-liquid phase transition and crossover behavior of critical properties from 3D to 2D. Fluid Phase Equilib. 300, 182–187.
Sondergeld, C.H., Newsham, K.E., Comisky, J.T., Rice, M.C., Rai, C.S., 2010. Petrophysical considerations in evaluating and producing shale gas resources. In: SPE Unconventional Gas Conference. February, Pittsburgh, Pennsylvania, USA, pp. 23–25.
Song, B., Ehlig-Economides, C., 2011. Rate-normalized pressure analysis for determination of shale gas well performance. In: North American Unconventional Gas Conference and Exhibition. June, The Woodlands, Texas, USA, pp. 14–16.
Suarez-Rivera, R., Chertov, M., Willberg, D., Green, S., Keller, J., 2012. Understanding permeability measurements in tight shales promotes enhanced determination of reservoir quality. In: SPE Canadian Unconventional Resources Conference, 30 October-1 November. Canada, Calgary, Alberta.
Van-Everdingen, A.F., Hurst, W., 1949. The application of the Laplace transformation to flow problems in reservoirs. J. Pet. Technol. 1, 305–324.
Van-Oort, E., 1994. A novel technique for the investigation of drilling fluid induced borehole instability in shales. In: Rock Mechanics in Petroleum Engineering Conference. August, Delft, Netherlands, pp. 29–31.
Wang, S., Feng, Q., Zha, M., Javadpour, F., Hu, Q., 2018. Supercritical methane diffusion in shale nanopores: effects of pressure, mineral types, and moisture content. Energy Fuel 32, 169–180.
Wang, J., Wang, B., Li, Y., Yang, Z., Gong, H., Dong, M., 2016a. Measurement of dynamic adsorption–diffusion process of methane in shale. Fuel 172, 37–48.
Wang, J., Yang, Z., Dong, M., Gong, H., Sang, Q., Li, Y., 2016b. Experimental and numerical investigation of dynamic gas adsorption/desorption–diffusion process in shale. Energy Fuel 30, 10080–10091.
Wu, K., Chen, Z., Li, X., Dong, X., 2016. Methane storage in nanoporous material at supercritical temperature over a wide range of pressures. Sci. Rep. 6, 1–10.
Wu, K., Li, X., Wang, C., Yu, W., Chen, Z., 2014. Apparent permeability for gas flow in shale reservoirs coupling effects of gas diffusion and desorption. In: Unconventional Resources Technology Conference. August, Denver, Colorado, USA, pp. 25–27.
Yang, Z., Dong, M., 2017. A new measurement method for radial permeability and porosity of shale. Pet. Res. 2, 178–185.
Yang, Z., Sang, Q., Dong, M., Zhang, S., Li, Y., Gong, H., 2015. A modified pressure-pulse decay method for determining permeabilities of tight reservoir cores. J. Nat. Gas Sci. Eng. 27, 236–246.
Yang, Z., Wang, W., Dong, M., Wang, J., Li, Y., Gong, H., Sang, Q., 2016. A model of dynamic adsorption-diffusion for modeling gas transport and storage in shale. Fuel 173, 115–128.
Yu, W., Sepehrnoori, K., Patzek, T.W., 2016. Modeling gas adsorption in Marcellus shale with Langmuir and BET isotherms. SPE J. 21, 589–600.
Yuan, W., Pan, Z., Li, X., Yang, Y., Zhao, C., Connell, L.D., Li, S., He, J., 2014. Experimental study and modelling of methane adsorption and diffusion in shale. Fuel 117, 509–519.
Zapata, Y., Sakhaee-Pour, A., 2016. Modeling adsorption-desorption hysteresis in shales: acyclic pore model. Fuel 181, 557–565.
Zarragoicoechea, G.J., Kuz, V.A., 2004. Critical shift of a confined fluid in a nanopore. Fluid Phase Equilib. 220, 7–9.
Zhai, Z., Wang, X., Jin, X., Sun, L., Li, J., Cao, D., 2014. Adsorption and diffusion of shale gas reservoirs in modeled clay minerals at different geological depths. Energy Fuel 28, 7467–7473.